# Clinical Translation of a Click-Labeled $^{18}$F-Octreotate Radioligand for Imaging Neuroendocrine Tumors

Suraiya R. Dubash[1], Nicholas Keat[2], Paola Mapelli[1], Frazer Twyman[1], Laurence Carroll[1], Kasia Kozlowski[1], Adil Al-Nahhas[3], Azeem Saleem[2], Mickael Huiban[2], Ryan Janisch[2], Andrea Frilling[4], Rohini Sharma[1], and Eric O. Aboagye[1]

*[1]Department of Surgery and Cancer, Imperial College London, London, United Kingdom; [2]Imanova Centre for Imaging Sciences, London, United Kingdom; [3]Department of Radiology/Nuclear Medicine, Imperial College Healthcare NHS Trust, London, United Kingdom; and [4]Department of Surgery, Imperial College Healthcare NHS Trust, London, United Kingdom*

We conducted the first-in-human study of $^{18}$F-fluoroethyl triazole [Tyr$^3$] octreotate ($^{18}$F-FET-βAG-TOCA) in patients with neuroendocrine tumors (NETs) to evaluate biodistribution, dosimetry, and safety. Despite advances in clinical imaging, detection and quantification of NET activity remains a challenge, with no universally accepted imaging standard. **Methods:** Nine patients were enrolled. Eight patients had sporadic NETs, and 1 had multiple endocrine neoplasia type 1 syndrome. Patients received 137–163 MBq (mean ± SD, 155.7 ± 8 MBq) of $^{18}$F-FET-βAG-TOCA. Safety data were obtained during and 24 h after radioligand administration. Patients underwent detailed whole-body PET/CT multibed scanning over 4 h with sampling of venous bloods for radioactivity and radioactive metabolite quantification. Regions of interest were defined to derive individual and mean organ residence times; effective dose was calculated with OLINDA 1.1. **Results:** All patients tolerated $^{18}$F-FET-βAG-TOCA with no adverse events. Over 60% parent radioligand was present in plasma at 60 min. High tumor (primary and metastases)-to-background contrast images were observed. Physiologic distribution was seen in the pituitary, salivary glands, thyroid, and spleen, with low background distribution in the liver, an organ in which metastases commonly occur. The organs receiving highest absorbed dose were the gallbladder, spleen, stomach, liver, kidneys, and bladder. The calculated effective dose over all subjects (mean ± SD) was 0.029 ± 0.004 mSv/MBq. **Conclusion:** The favorable safety, imaging, and dosimetric profile makes $^{18}$F-FET-βAG-TOCA a promising candidate radioligand for staging and management of NETs. Clinical studies in an expanded cohort are ongoing to clinically qualify this agent.

**Key Words:** neuroendocrine; $^{18}$F-fluroethyl [Tyr$^3$] octreotate analog; PET/CT imaging

**J Nucl Med 2016; 57:1207–1213**
DOI: 10.2967/jnumed.115.169532

Neuroendocrine tumors (NETs) are a heterogeneous group. Once thought of as rare tumors, the incidence and prevalence has risen over the last 3 decades, with figures from the National Cancer Institute's Surveillance, Epidemiology and End Results Database showing a 520% increase, now surpassing other gastrointestinal tumors and sharing the same incidence rates as tumors of the cervix and multiple myeloma (*1*). Gastroenteropancreatic NETs are the most common subtype, with the small bowel being the most frequent site (*1,2*).

Clinical presentation can vary and depends on the location of the tumor, presence of secretory products, and metastatic potential. Imaging is a pivotal part of the clinical workup when staging NET patients as well as aiding in treatment decisions and predicting response to therapy. Current anatomic imaging modalities, namely ultrasound, CT, MRI, and somatostatin receptor scintigraphy, fall short, with low sensitivity (82%–93%, 73%–83%, 89%–93%, and 89%, respectively) and operator dependence (ultrasound), thereby greatly underestimating the stage of disease (*3,4*).

$^{68}$Ga-DOTA-radiolabeled somatostatin analogs ($^{68}$Ga-labeled DOTATOC, DOTANOC, or DOTATATE) have been developed for use with PET; more recently, $^{64}$Cu-DOTATATE has also been developed although the isotope has a branching ratio of 0.175 and a 12.7-h half-life. $^{68}$Ga PET is far superior to somatostatin receptor scintigraphy in terms of resolution and sensitivity (*5–7*).

$^{18}$F-somatostatin analogs represent a cyclotron-generated alternative to $^{68}$Ga analogs. Thus, we developed a novel $^{18}$F-click-labeled octreotate radioligand, $^{18}$F-fluoroethyl triazole [Tyr$^3$] octreotate ($^{18}$F-FET-βAG-TOCA), for somatostatin receptor type 2 (SSTR-2) imaging (*8,9*). $^{18}$F-FET-βAG-TOCA (Fig. 1A), synthesized using a versatile 2-step method to label [Tyr3] octreotate via copper catalyzed azide-alkyne cycloaddition reaction (also known as click chemistry), was shown to be superior to other $^{18}$F-octreotate–labeled ligands and $^{68}$Ga-DOTATATE in preclinical models, with good tumor uptake and low nonspecific liver uptake (*8*).

We present the first-in-human biodistribution, dosimetry, and safety study of this radioligand in patients with NETs.

## MATERIALS AND METHODS

### Radiopharmaceutical Preparation

$^{18}$F-FET-βAG-TOCA was synthesized via the click reaction (*9*). Briefly, $^{18}$F-fluoride in a solution of oxygen-18–enriched water was transferred with a sweep of argon gas from the cyclotron target to the hot cell containing the automated module for radiochemistry. The $^{18}$F-fluoride was then trapped on an ion exchange cartridge (Sep-Pak QMA-carbonate Light Cartridge; Waters); released into the FASTLab reaction vessel (Waters), using 1.5 mL of a solution containing Kryptofix $K_{222}$ and $K_2CO_3$; and evaporated to dryness. A solution of 2-azidoethyl-p-toluenesulfonate (6 μL) in dry acetonitrile (1 mL) was added to the reaction vessel, and the solution was heated to 80°C for 15 min. The formed $^{18}$F-fluoroethyl azide was then distilled at 120°C into a vial containing a solution of copper sulphate (3.25 mg) in water

Received Nov. 12, 2015; revision accepted Jan. 29, 2016.
For correspondence or reprints contact: Eric O. Aboagye, Department of Surgery and Cancer, Imperial College London, London, U.K.
E-mail: eric.aboagye@imperial.ac.uk
Published online May 12, 2016.

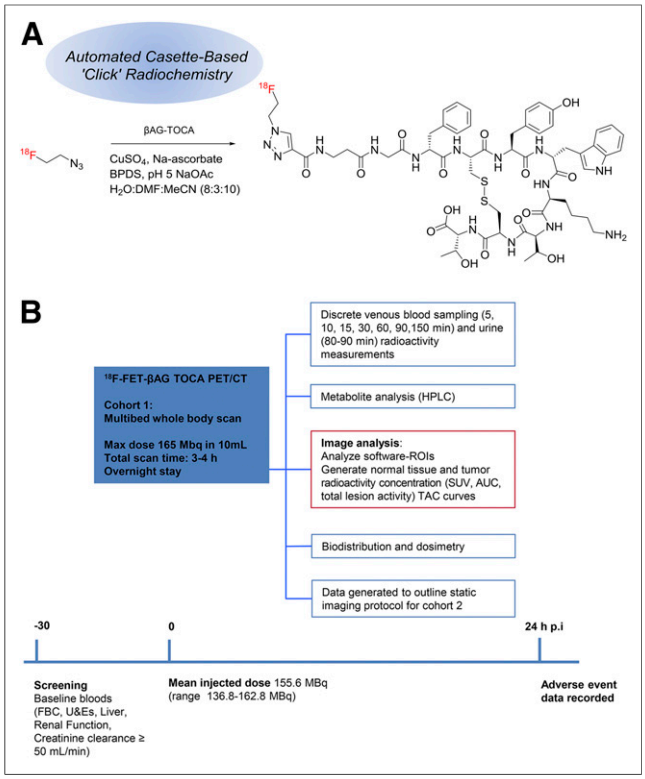


**FIGURE 1.** Chemical structure of $^{18}$F-FET-βAG-TOCA and study design. (A) Schematic diagram of chemical structure of $^{18}$F-FET-βAG-TOCA. pH 5, NaOAc $H_2O$; sodium acetate buffer (pH5), water; MeCN (8:3:10). (B) PET/CT study timeline. AUC = area under the curve; BPDS = bathophenanthrolinedisulfonate; $CuSO_4$ = copper (II) sulphate; DMF = dimethyl formamide; FBC = full blood count; Max = maximum; Na-ascorbate = sodium ascorbate; p.i. = after injection; ROIs = regions of interest; TAC = time–activity curves; U&Es = urea and electrolytes.

(25 μL) and a solution of βAG-TOCA (4 mg; obtained under contract from ABX [ABX Advanced Biochemical Compounds GmbH]) in *N,N*-dimethylformamide (50 μL). After distillation, 100 μL of a sodium ascorbate solution (56.7 mg in 2 mL of sodium acetate buffer) and 100 μL of a solution of bathophenanthroline disulfonic acid disodium salt trihydrate (192 mg) in 2 mL of water were added. The resulting mixture was mixed and allowed to react at room temperature for 5 min. The solution was then diluted with water and loaded onto semiprep high-performance liquid chromatography (HPLC) column (Jupiter Proteo [Phenomenex], 250 × 10 mm, 4 μm, 90 Å) for purification. The semiprep HPLC column was eluted at a 3 mL/min flow with a premixed solution consisting of water/acetonitrile/ethanol/concentrated HCl, 740/250/10/1. The product fraction eluting at the retention time corresponding to $^{18}$F-FET-βAG-TOCA was collected, diluted with 30 mL of ascorbic acid solution, and passed through a tC18 light Sep-Pak cartridge (Waters Corp.). After an initial Sep-Pak cartridge wash with sterile water, $^{18}$F-FET-βAG-TOCA was eluted off the cartridge with ethanol, 0.9% saline for injection, and water for injection to produce $^{18}$F-FET-βAG-TOCA formulated in 8 mL of maximum 12% (v/v) ethanol in 0.1% saline for injection. In the final step, the resulting formulation solution was filtered through a 0.2-μm sterile filter (Millex GV, Sterile, 0.22 μm; Millipore) into its final sterile container. The identity and purity (chemical and radiochemical purity) of the final product were determined by HPLC. Other quality control tests were performed according to European Pharmacopoeia guidelines.

### Patients

This was a prospective first-in-human study in 9 patients. All patients included were 18 y or older, with locally advanced or metastatic disease and a life expectancy 3 mo or more. Only patients who had a positive $^{68}$Ga-DOTATATE scan within the preceding 6 mo were enrolled. Patients who had received chemotherapy within 3 wk or radiotherapy within 4 wk and those with serious underlying medical illness or unable to tolerate scanning were excluded. Previous imaging was recorded to ascertain disease sites alongside histopathology, gut hormones, chromogranin levels (CgA and CgB), and Ki-67 index. The date and dose of the last octreotide/lanreotide injection were recorded where relevant. The Leeds East and Humberside Research Ethics Committee approved this study, and all subjects signed a written informed consent form. The study was conducted according to the Declaration of Helsinki. The administration of radioactivity was approved by the Administration of Radioactive Substances Advisory Committee, U.K. The Medicines and Health Care Products Regulatory Agency (U.K.) gave permission to administer the Investigational Medicinal Product (European Clinical Trials no. 2013-003152-20).

### Safety

Safety data were obtained during and 24 h after radioligand administration. Data recorded included vital signs (heart rate, blood pressure, respiratory rate, and body temperature); physical examination; cardiovascular, lung, abdomen, and neurologic examinations; electrocardiogram; and laboratory parameters (serum biochemistry, hematology, coagulation, and urinalysis). Any adverse events were recorded using the common toxicity criteria (version 4.03; http://www.eortc.be/services/doc/ctc/CTCAE_4.03_2010_0614_QuickReference_5 × 7.pdf).

### Image Acquisition

Images were acquired on a Biograph 6 TruePoint PET/CT scanner (with TrueV; extended field of view [Siemens]) with 21.6-cm axial and 60.5-cm transaxial fields of view. An attenuation CT scan of each patient was obtained before administration of $^{18}$F-FET-βAG-TOCA, from the vertex to the mid thigh (CT settings: tube potential, 130 kV; exposure, 15 effective mAs; pitch, 1.5; slice thickness, 5 mm; rotation time, 0.6 s; resulting in an effective dose of 2.5 mSv). This scan was then followed by a multibed whole-body PET scanning protocol on 6 occasions within a 4-h period. A break after the fourth emission scan allowed voiding to enhance radioligand clearance and was followed by a second CT and the last 2 multibed whole-body PET scans (Supplemental Table 1; supplemental materials are available at http://jnm.snmjournals.org).

All emission scans were reconstructed using the ordered-subsets expectation maximization algorithm (3 iterations and 21 subsets) with corrections for dead time, scatter, attenuation, and radioactive decay. Volumes of interest for as many of the possible International Commission on Radiological Protection (ICRP) 103 source organs were outlined (*10*), using the ANALYZE software package (version 11; Biomedical Imaging Resource, Mayo Clinic). All source organs were manually outlined on screen using a circular paint-brush of fixed diameter and width, by a single investigator to avoid any interobserver variation.

### Blood Activity Measurements

Discrete venous bloods and plasma (at 5, 10, 15, 30, 60, 90, and 150 min after injection) were obtained for radioactivity counting and metabolite analysis, as previously described (*8*).

### Data Analysis, Biodistribution, and Dosimetry

The mean non–decay-corrected $^{18}$F activity was obtained for the source organ regions of interest at each whole-body scan time, resulting in time–activity curves. The curves were decay-corrected to the midpoint of each whole-body scan to most closely represent the average activity distribution for the scan. To account for the activity remaining in the body at the end of the scan protocol, the time–activity curves were

extrapolated from the last whole-body scan with the simplification that radioactive decay would be the only significant change. The curves were converted to activity per organ using the volume of organs in ICRP 23 reference man (*11*) and normalized by the injected activity to give the fractional uptake in each organ as a function of time. These time–activity curves were trapezoidally integrated to generate organ residence times, the total number of disintegrations in each source organ per unit injected activity.

Bladder radioactivity, unlike other organs, was calculated, taking into account the bladder volume changes over the time course of the scan (*12–15*). The effective dose (ED) was calculated using, first, the mean residence time over all subjects for each organ and, second, residence times for individual subjects with OLINDA/EXM (version 1.1), which uses the organ weighting factors from ICRP 60 (*16*).

## RESULTS

### Patients

In this prospective study, 9 patients (6 women and 3 men) were recruited: 6 patients with gastroenteropancreatic NETs and 3 with lung NETs. One patient had known multiple endocrine neoplasia type 1 (MEN1) syndrome whereas the other tumors were sporadic. MEN1, an autosomal dominant hereditary syndrome for which patients develop pituitary, parathyroid, pancreatic, and adrenal tumors, is detected through familial screening. $^{68}$Ga-DOTA peptides allow the detection of NET lesions in MEN1 syndrome patients and can be used as an additional tool to CT scanning. The mean age and weight ± SD were 56 y ± 12.8 (range, 35–73 y) and 75.2 ± 11.8 kg (range, 66.3–91.2 kg), respectively. Study schedule (Fig. 1B), patient demographics, and clinical characteristics (Table 1) were summarized. The median CgA and CgB levels, reflecting in part the burden of disease (*17*), were 95 (range, 24–1,567) and 170 pmol/L (range, 58–1,328), respectively. Tumor staging and grading were in accordance with the European Neuroendocrine Tumor Society consensus classification systems (*18*). In our cohort of patients, 22% (2/9) were graded as G1 (≤2) and 78% (7/9) were G2.

### Safety

There were no adverse or clinically detectable pharmacologic events during the study or within 24 h after $^{18}$F-FET-βAG-TOCA injection. No significant changes in vital signs or the results of laboratory studies or electrocardiograms were observed.

### Radiopharmaceutical

$^{18}$F-FET-βAG-TOCA formulated for injection was obtained from fluoride in 6.2% ± 2.9% non–decay-corrected radiochemical yield (range, 2.0%–12.1%) within 100 min. Radiochemical purity was 100%, and specific radioactivity was 374 ± 124 GBq/μmol (range, 224–562 GBq/μmol). The mean (±SD) of the administered mass of $^{18}$F-FET-βAG-TOCA was 0.86 ± 0.26 μg (range, 0.52–1.32 μg). The mean administered activity was 155.7 ± 8 MBq (range, 137–163 MBq).

### Metabolite Analysis

The metabolism of $^{18}$F-FET-βAG-TOCA was analyzed using radio-HPLC (1200 series system; Agilent). Typical high-performance liquid chromatograms for subject 1 are illustrated in Figure 2. Over 60% of parent radioligand was detectable in plasma at 60 min, and over 30% of parent radioligand was detectable at 2.5 h (Supplemental Fig. 1). There was a rapid equilibration of radioactivity in blood, with a blood-to-plasma ratio of approximately 1.5. From the parent plasma data, the elimination half-lives of the distribution and terminal/elimination phase were calculated as 2.95 ± 0.87 and 15.87 ± 6.84 min, respectively (fit: $R^2$ range, 0.98–1.0), demonstrating rapid radioligand clearance from the blood compartment. The identity of the metabolites are presently unknown; no bone uptake was seen, thus precluding significant defluorination.

**TABLE 1**
Patient Clinical and Pathologic Characteristics

| Patient no. | Primary site | Age (y) | Sex | Grade | Metastatic | Ki-67 (%) (primary tumor histology) | Biomarker (pmol/L) | | Previous treatment |
|---|---|---|---|---|---|---|---|---|---|
| | | | | | | | CgA | CgB | |
| 1 | Small bowel | 53 | F | 2 | Liver, bone | >10 | 1,567 | 170 | Surgery/RFA/$^{177}$Lu*/octreotide |
| 2 | Small bowel | 73 | F | 1 | Paraaortic lymph nodes, left SCF | <1 | 962 | 558 | Surgery |
| 3 | Lung | 56 | F | 2 | Bone | <5 | 507 | 1,328 | Octreotide |
| 4 | Small bowel | 60 | F | 1 | Liver | <2 | 143 | 73 | Surgery/RFA/$^{177}$Lu |
| 5 | Lung | 68 | F | 2 | Mediastinal lymph nodes, bone | 17 | 47 | 58 | Surgery/RFA/$^{177}$Lu |
| 6 | Pancreas | 70 | M | 2 | None | 5 | 70 | 174 | Surgery |
| 7 | Pancreas | 53 | F | 2 | Liver, bone | 9 | 95 | 243 | Surgery/chemotherapy |
| 8 | Lung | 41 | M | 2 | Lung, liver | 12 | 24 | 126 | Surgery/RFA/$^{177}$Lu |
| 9 | Pancreas† | 35 | M | 2 | None | <5 | 49 | 124 | Surgery |

*$^{177}$Lu-DOTATATE (peptide receptor radionuclide therapy).
†MEN1.
RFA = radiofrequency ablation; SCF = supraclavicular fossa lymph node.

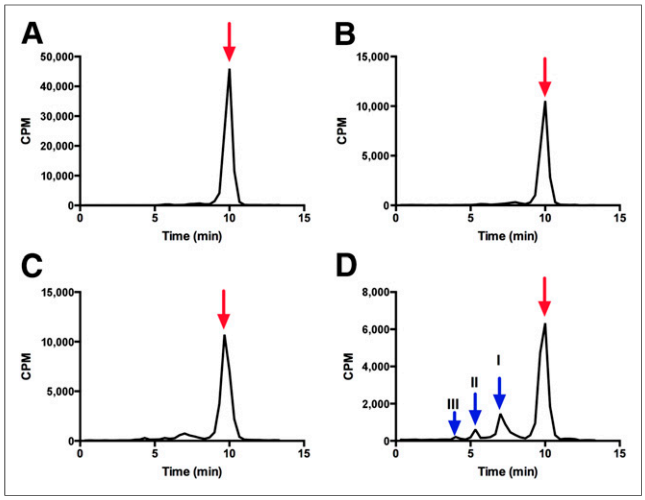


**FIGURE 2.** Metabolite analysis of $^{18}$F-FET-βAG-TOCA in patient 1. Typical high-performance liquid chromatogram of $^{18}$F-FET-βAG-TOCA in plasma at 5-, 30-, 60-, and 90-min time points (A, B, C and D, respectively). Red arrows indicate parent/unmetabolized $^{18}$F-FET-βAG-TOCA. Scaling of B, C, and D adjusted to allow for visualization of metabolite peaks I, II, and III (blue arrow). CPM = counts per minute.

### Image Quality

Images obtained with $^{18}$F-FET-βAG-TOCA PET/CT showed excellent contrast (Fig. 3). The image of patient 1, diagnosed with a small bowel NET and widespread metastases (bone, liver), shows avid uptake of $^{18}$F-FET-βAG-TOCA. Figure 4 shows images of a patient with known MEN1 syndrome and with lesions localized within the pancreas.

### Biodistribution

$^{18}$F-FET-βAG-TOCA–derived radioactivity was visually detectable in the vascular compartment, liver, spleen, and kidneys, within the first 6 min of radioligand injection. There were no significant differences in organ biodistribution between male and female patients (Fig. 5). Tissue time–activity curves generated for the main source organs are shown in Figure 6. Over the next 192 min, increased radioligand localization was seen in the gallbladder, spleen, and bladder. Physiologic uptake was also noted in the pituitary, salivary glands, and thyroid. The radioligand also showed high tumor uptake (Fig. 6C) and tumor-to-background contrast in all organs including the liver. Three lesions were chosen per patient where available, and in patients with multiple metastases, 3 lesions were chosen from different sites. In patients with multiple liver lesions only, 3 clearly visible lesions were identified and used for measurement of SUV.

The mean residence times in male and female patients are shown (Table 2). Overall, the radioligand was eliminated rapidly from most organs, leading to relatively short residence times and low/stable organ radioactivity within 60 min of radioligand injection. Bladder radioactivity was variable; an example of a bladder time–activity curve for subject 1 using the 3-parameter-fit model is illustrated in Supplemental Figure 2.

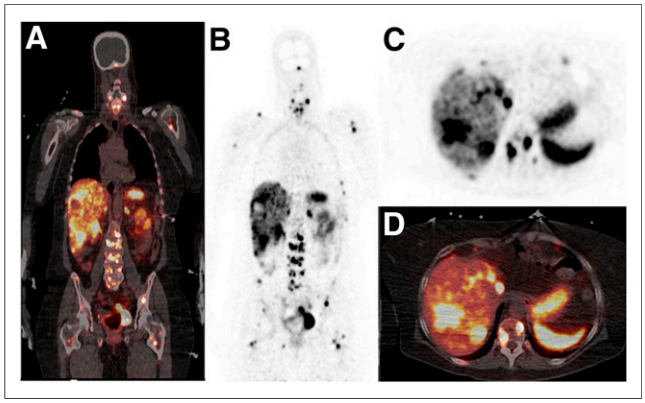


**FIGURE 3.** $^{18}$F-FET-βAG-TOCA PET/CT images and corresponding maximum-intensity-projection images in patient 1 (small bowel NET with widespread metastases in liver and bone). Sagittal images (A and B) and axial slices (C and D) showing widespread liver and bone metastases.

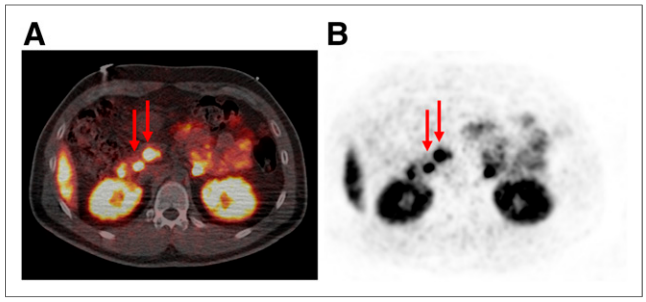


**FIGURE 4.** $^{18}$F-FET-βAG-TOCA PET/CT images and corresponding maximum-intensity-projection images in patient with MEN1 syndrome, with pancreatic NETs. (A and B) Axial slices showing multiple lesions within pancreas (red arrows).

### Dosimetry

The calculated ED using mean organ residence times over all 9 subjects was 0.029 mSv/MBq. When using time–activity curves for individual subjects, the calculated ED ranged from 0.022 to 0.032 mSv, giving an SD of 0.004 mSv. The estimated mean absorbed dose to all source organs assuming a 2-h bladder voiding scenario in individual patients (1–3) or all patients combined is shown in Figure 7. The organs that received the highest dose (mSv/MBq) in

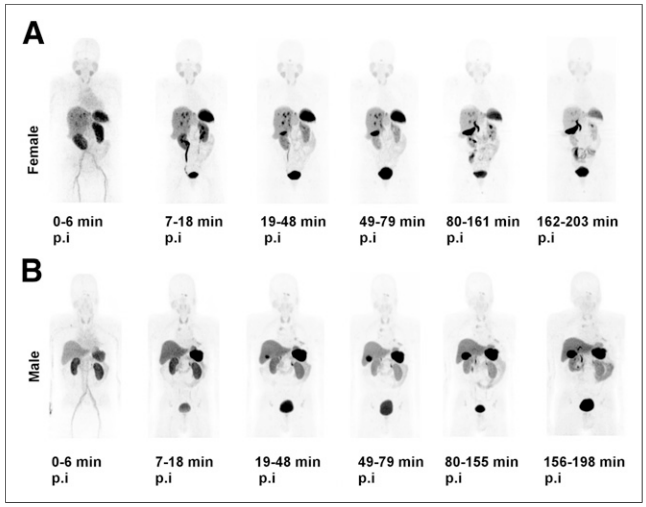


**FIGURE 5.** Time course biodistribution of $^{18}$F-FET-βAG-TOCA in male and female patients. Maximum-intensity-projection images of $^{18}$F-FET-βAG-TOCA in female patient with liver metastases (A) and male patient with lung NET (B). p.i. = after injection.

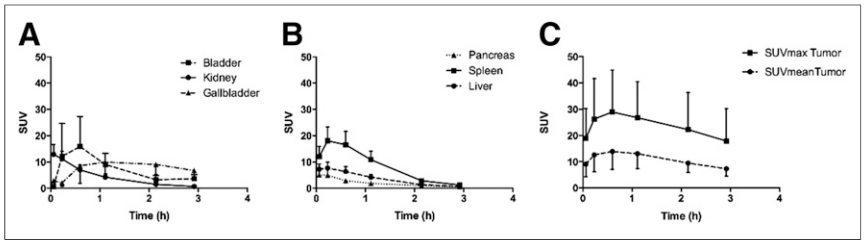


**FIGURE 6.** Mean decay-corrected time–activity curves for source organs and tumors. (A and B) $SUV_{mean}$ for bladder, kidneys, gallbladder, pancreas, spleen, and liver. (C) $SUV_{mean}$ and $SUV_{max}$ for tumors (maximum of 3 lesions chosen per patient).

descending order were the gallbladder wall (0.149 ± 0.007), spleen (0.117 ± 0.036), stomach wall (0.076 ± 0.02), liver (0.066 ± 0.009), kidneys (0.065 ± 0.011), and urinary bladder (0.051 ± 0.015).

## DISCUSSION

$^{18}$F-FET-βAG-TOCA, a SSTR-2 targeting $^{18}$F radioligand, has been shown in this first-in-human study to be safe and well tolerated. Good-manufacturing-practice-compliant $^{18}$F-FET-βAG-TOCA was produced on an automated platform; synthesis time of $^{18}$F-FET-βAG TOCA, using the click reaction (*9*), was shown to be shorter than other $^{18}$F-octreotate analogs and resulted in reasonable radioligand yields (*19*). $^{18}$F-FET-βAG-TOCA had acceptable metabolic stability with little or no defluorination. Intact parent radioligand was detectable in plasma by HPLC throughout the study; radioactivity in urine comprised up to 90% of parent radioligand at 90 min after injection (data not shown).

Future users of this radioligand should be cognizant of physiologic localization. Low-level physiologic localization was seen in the pituitary, salivary glands, thyroid, and spleen, and elimination via the gallbladder increased over time. Rapid distribution to the liver was noted, but over time there was gradual elimination of radioligand in this organ and background activity proved to be less than other previously described $^{18}$F-octreotate–based radioligands (*19,20*). This is in keeping with preclinical studies in mice. $^{18}$F-FET-βAG-TOCA was selected from a library of compounds mainly because of its low level of uptake in the liver—a common site for metastases in neuroendocrine tumors—while retaining reasonably high binding affinity comparable to ($^{18}$F-AIF-NOTA-OC) or higher than existing clinically applicable radioligands ($^{68}$Ga-DOTATATE) (*8,9*).

The main pharmacokinetic difference between $^{18}$F-FET-βAG-TOCA and $^{68}$Ga-emitting somatostatin radioligands relates to the highest absorbed dose received by source organs, in which, in descending order, the spleen, bladder, kidneys, and liver receive the highest dose with $^{68}$Ga-emitting somatostatin radioligands. In comparison, for $^{18}$F-FET-βAG-TOCA, the gallbladder received the highest absorbed dose. This is to be expected because $^{18}$F-FET-βAG-TOCA had both renal and biliary elimination, whereas $^{68}$Ga-based ligands have predominantly renal elimination (*21–23*). In our cohort of patients with liver metastases, the tumor-to-background ratio for $^{18}$F-FET-βAG-TOCA in the liver (4.23 ± 2.69) was broadly similar to that reported for $^{68}$Ga-DOTANOC (3.4 ± 2.3), $^{68}$Ga-DOTATOC (2.8 ± 1.6), and $^{68}$Ga-DOTATATE (2.0; interquartile range, 1.4–2.7) (*24–26*).

The dosimetry of $^{18}$F-FET-βAG-TOCA was similar to other $^{18}$F-based radioligands. The mean ED was found to be 0.029 ± 0.004 mSv/MBq, which is comparable to the ED of $^{18}$F-FDG (0.019 mSv/MBq) (*27*). Radiation safety of $^{18}$F-FET-βAG-TOCA was inferred from the organ absorbed dose estimates obtained from our study; all values were within the limits suggested by the U.S. Food and Drug Administration Code of Federal regulation Title 21, part 361.1.

Although ours was a small cohort of patients, we observed no trend between SUVs and blood biomarkers or grade of tumors. Patient 1, for instance, was found to have a high tumor burden reflected by high chromogranin CgA and CgB levels and high SUV of lesions within the liver, bone, and bowel; however, patient 3 (lung NET) showed low tumor burden with low SUV, but CgA and CgB levels were high. Additionally, patient 7 (pancreatic NET) was found to have low levels of CgA despite having widespread liver metastases on $^{18}$F-FET-βAG-TOCA PET/CT. This lack of correlation

**TABLE 2**
Mean Residence Times (MBq·h/MBq) of $^{18}$F-FET-βAG-TOCA for Different Organs in Male ($n$ = 3) and Female ($n$ = 6) Subjects

| Organ | Men | | Women | |
|---|---|---|---|---|
| | Mean | SD | Mean | SD |
| Adrenals* | 0.002 | 0.0002 | 0.003 | 0.0008 |
| Brain | 0.006 | 0.001 | 0.007 | 0.001 |
| Breasts | | | 0.004 | 0.001 |
| Cortical bone | 0.049 | 0.002 | 0.040 | 0.016 |
| Gallbladder† | 0.110 | | 0.072 | 0.019 |
| Heart contents | 0.029 | 0.014 | 0.019 | 0.005 |
| Heart wall | 0.020 | 0.010 | 0.013 | 0.004 |
| Kidneys | 0.088 | 0.007 | 0.089 | 0.026 |
| Liver | 0.478 | 0.073 | 0.089 | 0.084 |
| Lungs | 0.063 | 0.009 | 0.067 | 0.025 |
| Lower large intestine | 0.012 | 0.002 | 0.019 | 0.011 |
| Muscle | 0.709 | 0.154 | 0.600 | 0.154 |
| Ovaries‡ | | | 0.0005 | 0.00004 |
| Pancreas | 0.017 | 0.006 | 0.010 | 0.0035 |
| Red marrow | 0.028 | 0.004 | 0.050 | 0.032 |
| Small intestine | 0.094 | 0.065 | 0.121 | 0.055 |
| Stomach | 0.005 | 0.029 | 0.066 | 0.222 |
| Spleen | 0.122 | 0.019 | 0.097 | 0.026 |
| Testes | 0.001 | 0.0002 | | |
| Thyroid | 0.001 | 0.0003 | 0.0008 | 0.0003 |
| Upper large intestine | 0.026 | 0.004 | 0.028 | 0.014 |
| Urinary bladder¶ | 0.075 | 0.019 | 0.101 | 0.028 |
| Uterus | | | 0.006 | 0.001 |
| Remainder | 0.523 | 0.250 | 0.628 | 0.025 |

*Adrenal glands could not be visualized in 3 subjects.

†Gallbladder surgically removed in 5 subjects (1 male subject had gallbladder in situ).

‡Ovaries could not be visualized in 1 subject because of postmenopausal atrophy, and 2 subjects had previous hysterectomy and bilateral salpingo-oophorectomy.

¶Urinary bladder mean residence time is for 2-h voiding model.

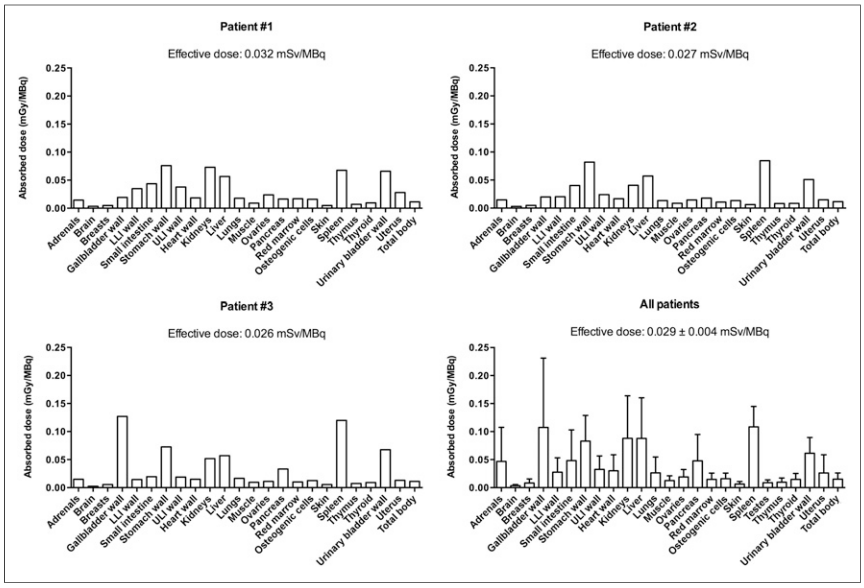


**FIGURE 7.** Biodistribution and dosimetry of $^{18}$F-FET-βAG-TOCA. Multibed whole-body PET scanning over 192 min was used to determine absorbed doses per unit administered activity (mGy/MBq) of major organs and tissues for each patient (first 3 patients are shown). Organ absorbed doses in all patients are shown with mean effective dose ± SD. LLI = lower large intestine; ULI = upper large intestine.

between imaging and biomarkers has also been highlighted in other studies (*28,29*) and suggests that additional multianalyte biomarkers such as circulating NET gene transcripts should be considered in the future (*30*).

The MEN1 syndrome–positive patient in our study had previous pituitary surgery and therefore showed no uptake within this region (physiologic or pathologic). Imaging with $^{18}$F-FET-βAG-TOCA detected multiple NETs within the pancreas, and as expected there were no differences in SUVs of lesions between the MEN1-positive patient and other patients with gastroenteropancreatic NETs or lung NETs.

$^{18}$F-FET-βAG-TOCA has shown initial promise with its ease of synthesis, high production yield, and accessibility for large multicenter studies, and clinical studies in an expanded cohort, with a single static whole-body imaging protocol based on this study, are currently ongoing to clinically qualify the ligand in patients with NET, by direct comparison with $^{68}$Ga-DOTATATE PET/CT. The potential of this SSTR-specific radioligand, with high specificity for SSTR-2, highlights the possibility for use both in diagnosis and in treatment planning, an attractive option in NET patients. This concept of theranostics (therapies that combine diagnostic and therapeutic capabilities into a single agent) in nuclear medicine has gained popularity and is one step forward in achieving a personalized medicine approach in NET patients. Although this concept applies directly to $^{68}$Ga-DOTA radioligands (*31*), it is envisaged that the $^{18}$F variant can be used, indirectly, to personalize similar therapies.

## CONCLUSION

We report a click $^{18}$F-radiolabeled octreotate PET imaging radiopharmaceutical with appropriate safety, dosimetry, and distribution properties, which highlights tumor lesions with high contrast. With the range of treatment modalities available in the management of NETs, the use of an optimal imaging modality, together with blood biomarkers in the clinic, is of great importance in the therapeutic decision-making process of NET patients.

## DISCLOSURE

The costs of publication of this article were defrayed in part by the payment of page charges. Therefore, and solely to indicate this fact, this article is hereby marked "advertisement" in accordance with 18 USC section 1734. This work was supported by the U.K. Medical Research Council grant MR/J007986/1, Experimental Cancer Medicine Centres grant C37/A7283, and National Institute for Health Research (NIHR) Biomedical Research Centre award to Imperial College Healthcare NHS Trust and Imperial College London. GE Healthcare provided in-kind contribution to support radiochemistry on the FASTlab platform. No other potential conflict of interest relevant to this article was reported.

## ACKNOWLEDGMENTS

We thank the patients who participated in the trial, the staff of Imanova Ltd., and the staff of NIHR/Wellcome Trust Imperial Clinical Research Facility for their support of the trial.

## REFERENCES

1. Lawrence B, Gustafsson BI, Chan A, Svejda B, Kidd M, Modlin IM. The epidemiology of gastroenteropancreatic neuroendocrine tumors. *Endocrinol Metab Clin North Am.* 2011;40:1–18.
2. Yao JC, Hassan M, Phan A, et al. One hundred years after "carcinoid": epidemiology of and prognostic factors for neuroendocrine tumors in 35,825 cases in the United States. *J Clin Oncol.* 2008;26:3063–3072.
3. Sundin A, Vullierme MP, Kaltsas G, Plockinger U, Mallorca Consensus Conference participants, European Neuroendocrine Tumor Society. ENETS consensus guidelines for the standards of care in neuroendocrine tumors: radiological examinations. *Neuroendocrinology.* 2009;90:167–183.
4. Clift AK, Faiz O, Al-Nahhas A, et al. Role of staging in patients with small intestinal neuroendocrine tumours. *J Gastrointest Surg.* 2016;20:180–188.
5. Kowalski J, Henze M, Schuhmacher J, Macke HR, Hofmann M, Haberkorn U. Evaluation of positron emission tomography imaging using [$^{68}$Ga]-DOTA-D Phe (1)-Tyr(3)-Octreotide in comparison to [$^{111}$In]-DTPAOC SPECT: first results in patients with neuroendocrine tumors. *Mol Imaging Biol.* 2003;5:42–48.
6. Gabriel M, Decristoforo C, Kendler D, et al. $^{68}$Ga-DOTA-Tyr3-octreotide PET in neuroendocrine tumors: comparison with somatostatin receptor scintigraphy and CT. *J Nucl Med.* 2007;48:508–518.
7. Ruf J, Heuck F, Schiefer J, et al. Impact of multiphase $^{68}$Ga-DOTATOC-PET/CT on therapy management in patients with neuroendocrine tumors. *Neuroendocrinology.* 2010;91:101–109.
8. Leyton J, Iddon L, Perumal M, et al. Targeting somatostatin receptors: preclinical evaluation of novel $^{18}$F-fluoroethyltriazole-Tyr3-octreotate analogs for PET. *J Nucl Med.* 2011;52:1441–1448.
9. Iddon L, Leyton J, Indrevoll B, et al. Synthesis and in vitro evaluation of [$^{18}$F] fluoroethyl triazole labelled [Tyr3]octreotate analogues using click chemistry. *Bioorg Med Chem Lett.* 2011;21:3122–3127.
10. International Commission on Radiological Protection (ICRP). The 2007 recommendations of the International Commission on Radiological Protection. ICRP publication 103. *Ann ICRP.* 2007;37:1–332.
11. International Commission on Radiological Protection (ICRP). Task Group on Reference Man. *Report of the Task Group on Reference Man: A Report*. Oxford, U.K.: Pergamon Press; 1975.
12. Thomas SR, Stabin MG, Chen CT, Samaratunga RC. MIRD pamphlet no. 14 revised: a dynamic urinary bladder model for radiation dose calculations. Task Group of the MIRD Committee, Society of Nuclear Medicine. *J Nucl Med.* 1999;40:102S–123S.
13. Graham MM, Peterson LM, Link JM, et al. Fluorine-18-fluoromisonidazole radiation dosimetry in imaging studies. *J Nucl Med.* 1997;38:1631–1636.

14. Stabin MG, Sparks RB, Crowe E. OLINDA/EXM: the second-generation personal computer software for internal dose assessment in nuclear medicine. *J Nucl Med.* 2005;46:1023–1027.
15. Challapalli A, Sharma R, Hallett WA, et al. Biodistribution and radiation dosimetry of deuterium-substituted $^{18}$F-fluoromethyl-[1, 2-2H4]choline in healthy volunteers. *J Nucl Med.* 2014;55:256–263.
16. International Commission on Radiological Protection (ICRP). Recommendations of the International Commission on Radiological Protection. ICRP publication 60. *Ann ICRP.* 1990:21.
17. Zatelli MC, Torta M, Leon A, et al. Chromogranin A as a marker of neuroendocrine neoplasia: an Italian multicenter study. *Endocr Relat Cancer.* 2007;14:473–482.
18. Rindi G, Kloppel G, Couvelard A, et al. TNM staging of midgut and hindgut (neuro) endocrine tumors: a consensus proposal including a grading system. *Virchows Arch.* 2007;451:757–762.
19. Meisetschläger G, Poethko T, Stahl A, et al. Gluc-Lys([$^{18}$F]FP)-TOCA PET in patients with SSTR-positive tumors: biodistribution and diagnostic evaluation compared with [$^{111}$In]DTPA-octreotide. *J Nucl Med.* 2006;47:566–573.
20. Wieder H, Beer AJ, Poethko T, et al. PET/CT with Gluc-Lys-([$^{18}$F]FP)-TOCA: correlation between uptake, size and arterial perfusion in somatostatin receptor positive lesions. *Eur J Nucl Med Mol Imaging.* 2008;35:264–271.
21. Pettinato C, Sarnelli A, Di Donna M, et al. $^{68}$Ga-DOTANOC: biodistribution and dosimetry in patients affected by neuroendocrine tumors. *Eur J Nucl Med Mol Imaging.* 2008;35:72–79.
22. Hartmann H, Zophel K, Freudenberg R, et al. Radiation exposure of patients during Ga-DOTATOC PET/CT examinations [in German]. *Nuklearmedizin.* 2009;48:201–207.
23. Walker RC, Smith GT, Liu E, Moore B, Clanton J, Stabin M. Measured human dosimetry of $^{68}$Ga-DOTATATE. *J Nucl Med.* 2013;54:855–860.
24. Prasad V, Baum RP. Biodistribution of the Ga-68 labeled somatostatin analogue DOTA-NOC in patients with neuroendocrine tumors: characterization of uptake in normal organs and tumor lesions. *Q J Nucl Med Mol Imaging.* 2010;54:61–67.
25. Kroiss A, Putzer D, Decristoforo C, et al. $^{68}$Ga-DOTA-TOC uptake in neuroendocrine tumour and healthy tissue: differentiation of physiological uptake and pathological processes in PET/CT. *Eur J Nucl Med Mol Imaging.* 2013;40:514–523.
26. Wild D, Bomanji JB, Benkert P, et al. Comparison of $^{68}$Ga-DOTANOC and $^{68}$Ga-DOTATATE PET/CT within patients with gastroenteropancreatic neuroendocrine tumors. *J Nucl Med.* 2013;54:364–372.
27. International Commission on Radiological Protection (ICRP). Radiation dose to patients from radiopharmaceuticals (addendum 2 to ICRP publication 53). *Ann ICRP.* 1998;28:1–126.
28. Namwongprom S, Wong FC, Tateishi U, Kim EE, Boonyaprapa S. Correlation of chromogranin A levels and somatostatin receptor scintigraphy findings in the evaluation of metastases in carcinoid tumors. *Ann Nucl Med.* 2008;22:237–243.
29. Bodei L, Kidd M, Modlin IM, et al. Gene transcript analysis blood values correlate with $^{68}$Ga-DOTA-somatostatin analog (SSA) PET/CT imaging in neuroendocrine tumors and can define disease status. *Eur J Nucl Med Mol Imaging.* 2015;42:1341–1352.
30. Oberg K, Modlin IM, De Herder W, et al. Consensus on biomarkers for neuroendocrine tumour disease. *Lancet Oncol.* 2015;16:e435–e446.
31. Hörsch D, Kulkarni HR, Baum RP. Theranostics: clinical aimshots in surgical warfare against well-differentiated neuroendocrine neoplasms. *Ann Transl Med.* 2014;2:1–8.